Sonoluminescence and phase diagrams of single bubbles at low dissolved air concentrations

G. Simon,[1] I. Csabai,[2] Á. Horváth,[1] and F. Szalai[3]
[1]*Department of Atomic Physics, Eötvös Loránd University, H-1117 Budapest, Hungary*
[2]*Department of Physics of Complex Systems, Eötvös Loránd University, H-1117 Budapest, Hungary*
[3]*Computer and Automation Research Institute, Hungarian Academy of Sciences, P.O. Box 63, H-1518 Budapest, Hungary*
(Received 3 January 2000; revised manuscript received 11 September 2000; published 10 January 2001)

We studied experimentally the dependence of light emission and phase space boundaries of air bubbles in water on the level of degassing down to low partial pressures of 15 mmHg. We found that the maximum obtainable light intensity increased monotonically by lowering the concentration of dissolved air in water. We also present a new technique to obtain the acoustic pressure (P_a) and ambient radius (R_0) parameters, based on the information provided by the timing of the flashes in the acoustic cycle. Using this technique we give phase diagrams of the bubble in the (R_0, P_a) and (P_a, gas concentration) space, and discuss the parametric dependence of the light intensity. The resulting power-law dependence of the relative intensity normalized by the ambient volume of the bubble on the expansion ratio indicates that more extreme conditions are attainable inside a bubble at dissolved air concentration of 15 mmHg than at 150 mmHg.

DOI: 10.1103/PhysRevE.63.026301 PACS number(s): 47.55.Dz, 43.25.+y, 78.60.Mq

I. INTRODUCTION

Single bubble sonoluminescence (SBSL) is a phenomenon where an acoustically levitated gas bubble emits ultrashort flashes of light. Since its discovery [1] many aspects of the phenomenon has been studied experimentally as well as theoretically, such as the duration [2], the intensity and the spectrum [3] of the light pulses and their dependence on experimental parameters [4,5]. Some of the most successful light emission theories that are consistent with the experiments are given in Ref. [6].

An acoustically driven bubble exhibit sonoluminescence (SL) only in a limited part of the ($P_a, R_0, C_i/C_0$) parameter space [7], where P_a is the acoustic pressure amplitude, R_0 is the ambient radius, and C_i/C_0 is the ratio of dissolved air concentration set during water preparation to the equilibrium air concentration at room temperature and an ambient pressure of 1 atm. The actual path of the bubble in the ($P_a, R_0, C_i/C_0$) parameter space is specified by rectified diffusion [8] and shape instability thresholds [9]. Increasing the excitation pressure from zero makes the bubble go through different phases whose boundaries depend on the above parameters. At the most commonly used $C_i/C_0=0.2$ the general picture is the following. At low excitation the radial oscillations of the bubble are small, and nearly harmonic. In this regime the net mass transfer of air due to diffusion in each acoustic cycle is directed from the bubble towards the liquid, thus the bubble eventually dissolves in the water. At higher acoustic pressures the above process reverses, which results in the growth of the bubble. The bubble grows from cycle to cycle until it reaches the parametric shape instability threshold [9], then it breaks up and starts to grow again. In this phase the bubble seen to be ''jittering'' or ''dancing.'' On the boundary between these phases the bubble can be in an unstable diffusive equilibrium, where the net mass transfer in and out of the bubble equals zero. At sufficiently large pressure amplitudes the content of the bubble changes due to chemical reactions, leading to the accumulation of the chemically inert argon inside [10] (air contains about 1% of argon). This process was termed as the ''dissociation hypothesis'' and was later confirmed using several different experimental approaches [11–13]. In short the accumulation occurs because at high forcing the temperature of the gas will be high enough during the collapses, so that molecular compounds can dissociate, and form reaction products which will dissolve in the water. The process also leads to the existence of a stable equilibrium phase (observed by many researchers [11,12]) where the growth by rectified diffusion is balanced by the loss of mass due to chemical reactions. At the upper end of this phase the bubble contains almost exclusively just argon, which is also reflected in the decreased value of its ambient radius [4]. When further increasing the excitation, the bubble starts to emit light until an upper threshold is reached, which leads to its destruction. During the sonoluminescent phase the bubble is in a stable diffusive equilibrium and seems to be well described by Eller–Flynn theory [8] using C_i/C_0 values corresponding to the inert gas concentrations [7,14,12]. Previous studies by Gaitan and Holt [7] measured these phases in (P_a, R_0) parameter space at constant C_i/C_0 values of 0.2, 0.45, and 0.5. In this paper we concentrate on $C_i/C_0<0.2$ [15], but for comparison purposes we also made measurements at $C_i/C_0=0.2$ and 0.5. Our experimental setup did not allow the direct measurements of P_a and R_0, but in Sec. IV B we show that using the direct consequences of the dissociation hypothesis it is possible to obtain these parameters for stable sonoluminescing bubbles by measuring the timing of the flashes in the acoustic period [16]. The standard way to obtain these parameters is to use Mie scattering [17], or direct imaging of the bubble [18].

II. EXPERIMENTAL APPARATUS AND MEASUREMENT TECHNIQUES

In the measurements we used a sealed cylindrical resonator in many aspects similar to the one described in Ref. [5] (see their Fig. 4). It consists of two circular aluminum plates of thickness 1.5 mm, flat silicon O rings for sealing, ceramic

piezoelectric PZT transmitters glued on the top and the bottom of the plates, and a 1.5 mm thick pyrex glass cylinder. The plates were pushed against the cylinder by means of three screws. The best Q value of the resonator was obtained if the screws were tightened just enough to avoid the leakage of water at the O rings. The water temperature was measured by a thermocouple. Bubbles were created by letting an electric current run through a tiny tungsten wire, and thus boil the water locally. The current was made adjustable to create bubbles efficiently at any degree of degassing of the water.

The preparation of the water samples with a given air concentration were made at room temperature in a reservoir connected to a pressure gauge and a vacuum pump and to the resonator through a filling tube. To set a desired concentration first the partial pressure of air was reduced by pumping to a level calculated from Henry's law, correcting for the vapor pressure of water. After this the pump was detached by vacuum valves leaving the air–water system completely closed. To accelerate the establishment of thermodynamic equilibrium between the two media the water was mixed by means of a magnetic stirrer. The process could be monitored by measuring the partial pressure of air, which showed slight increase in the beginning due to the amount diffused out from the water and later saturated at a constant value (≈ 5 mmHg higher than the preset value), implying that the air–water system reached thermodynamic equilibrium. Even though the equilibrium already established typically in less than 20 minutes, altogether we stirred for 30 minutes in each case. The dissolved air concentrations reported in this paper were calculated from the final values of the partial pressures. After the degassing process the reservoir was brought to atmospheric pressure, in order to be able to fill the resonator using gravity flow through the filling tube. The filling took typically 2 minutes, during which some air might diffuse back into the water, however measurements with a digital O_2 concentration-meter revealed that within the 5% accuracy of the O_2 meter the concentration in the resonator matched the desired values [19].

The experimental configuration consisted of a photomultiplier tube (PMT) (GAMMA Type:ND-319/G) to detect the light emission and a 32 MHz digital oscilloscope (Velleman PCS32) linked to a PC to record the timing and the amplitude of the PMT signal and also of the monitored electric signal of the PZT transmitters. The PMT has a built-in signal shaping preamplifier circuit which transforms a fast input signal (such as a SL flash) uniformly to a negative output spike with 1 μs full width at half-maximum (FWHM), so the number of detected photons from a flash in the wavelength interval of 300–600 nm could be taken to be proportional to the amplitude of the output signal. The phase space boundaries were observed visually by back-lighting the bubble. Throughout the whole measurement we used the monitored electric signal on the piezo transmitters as a signal which is proportional to the acoustic pressure amplitude P_a. The measurements were carried out at an excitation frequency of 23 354 Hz, a water temperature of 23.5 ± 1 degrees, an ambient pressure of 1020 ± 2 mbar, and at degassing to partial pressures of 15, 38, 76, 114, 152, 233, 382 mmHg. The corresponding C_i/C_0 parameters 0.02, 0.05, 0.1, 0.15, 0.2, 0.31, 0.5 are calculated from the partial pressures using Henry's law: $C_i/C_0 = P_i/P_0^*$, where P_0^* is the standard 1 atm. At each degassing level for at least two runs the excitation was increased slowly from zero above the upper threshold of SL, and the electric signal amplitudes corresponding to the phase space boundaries were noted down. After this the SL phase was remeasured, where we recorded the output of the PMT and the monitored electric signal, except at the two highest partial pressures. We did not make PMT measurements at 233 mmHg, and 382 mmHg, because the fluctuations in the intensity and in the timing of the flashes were already too high in this parameter region, so the data could not be represented by snapshots of the PMT signal. At lower partial pressures the precision was limited only by the performance of the data acquisition software supplied with the digital scope to ± 0.3 μs for the detection of the timing of the flashes and to ± 0.005 V for the monitored electric signal. The intensity fluctuations are estimated to be less then 10%.

III. EXPERIMENTAL RESULTS INDEPENDENT OF THE FITTING TECHNIQUE

Some qualitative features and trends of the bubble's response can already be recognized from Fig. 1, which shows the raw experimental data before the application of the fitting technique. Here the ordinate shows the monitored electric signal of the PZT transmitters. Multiplied by 1000 this gives the true voltage amplitudes which were necessary to subject onto the PZT transmitters in order to excite the corresponding states of the bubble. The lowest set of symbols (+) represent the line of diffusive equilibrium which was found to be unstable for $C_i/C_0 \geqslant 0.1$. At excitation amplitudes below this line the bubbles were observed to dissolve, above it to grow and exhibit ''dancing'' motion. We note that the ''dancing'' motion was more prominent at high air concentrations, while at the two lowest partial pressures it was hard to tell by eye if the bubble was ''jittering'' at all or it was stable. The other two sets of symbols are the lower ($\bigcirc$) and upper ($\times$) thresholds of the light emission. The figure shows that the size of the region where the bubble grows tends to decrease towards low partial pressures, while the size of the sonoluminescent phase increases. Below the lower SL threshold we also observed the stable non-light-emiting phase, but the excitation amplitudes corresponding to this phase space boundary were not noted down, because the transition from ''jittering'' to stable behavior was not sharp enough for the eye to clearly identify an exact threshold. Another difference in the bubble's response at the two lowest partial pressures is that sometimes the bubbles observed to disappear completely before reaching the SL phase and thus in these cases the lower SL threshold could be identified only by creating a new bubble in the SL phase and subsequently decreasing the excitation until the light emission (and also the bubble) disappeared. At partial pressure of 385 mmHg ($C_i/C_0 = 0.5$) in agreement with Ref. [7] the ''jittering'' was observed also in the SL phase, indicating unstable sonoluminescence.

The maximum detected light intensity (at a given gas concentration) is also found to increase monotonically with low-

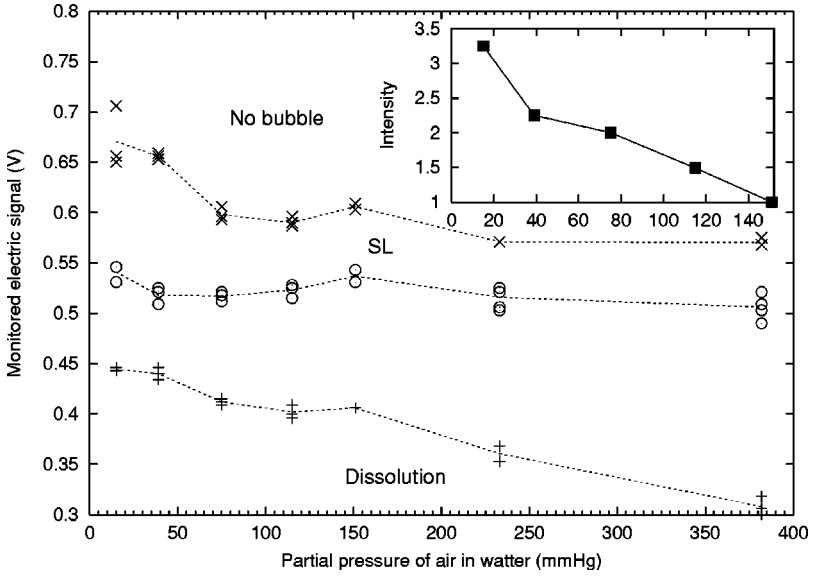

FIG. 1. Raw experimental data for excitation amplitudes of phase space boundaries as a function of partial pressure overhead of air above water. The inset shows the maximum obtained light intensity at each partial pressure normalized to the value obtained at 150 mmHg. These maximum values correspond to bubbles which perished in less than 5 seconds.

ering the air concentration down to 15 mmHg (see the inset of Fig. 1). This result seems to disagree with the previous measurements of Hiller *et al.* [20] using 1% argon in nitrogen mixtures, and Chow *et al.* [21] using 1% argon in oxygen mixtures. For comparison see Figs. 23 and 24 in Ref. [5] or the original references. Their data indicate that the maximum obtainable light intensity has a peak at about 130 and 100 mmHg, respectively, and decreases by an order of magnitude as the gas concentration approaches zero. Since all of these measurements used 1% argon, and in SL phase, according to Refs. [10–12], only the inert gas content which is relevant, one would expect an agreement if all the other experimental conditions are the same. However, there are several differences which make a direct comparison difficult. In the data of Hiller *et al.* the maximum light intensity corresponds to a value which was stable for more than a minute (see the caption of Fig. 2 in Ref. [20]), while in our case we defined the maximum as the value at which the bubble perished in less than 5 seconds. This later definition allows for higher excitation and thus higher light intensities before the destruction of the bubble. Another difference is that Hiller *et al.* used a resonator with acrylic walls, which passes light wavelengths longer than 380 nm, while the ultraviolet cutoff of our glass cylinder is about 300 nm [22]. Since in the spectrum of a SL flash the intensity increases strongly towards the 200 nm cutoff of water [3], this again results in different PMT signals even at otherwise identical conditions. The discrepancy due to this fact is expected to be bigger at low gas concentrations, where the bubble dynamics is characterized by higher expansion ratios, and lower ambient radius values, which would likely result in higher internal temperatures and more ultraviolet spectra. Finally the location of the extinction threshold in the (P_a, R_0) parameter space which determines the maximum intensities is likely not universal, but may be sensitive to the actual experimental conditions. These can include the ambient pressure, temperature, changes in the material properties of the liquid due to impurities, or the geometry and acoustic properties of the resonator. As a physical mechanism where even these two last mentioned properties can play a role one can think of the influence of the shockwave refocused from the resonator walls, launched by the bubble at the collapse [24]. As yet it is unclear which of the above-mentioned possibilities are the dominant ones to explain the difference between these results, thus our conclusion on this point is that for a satisfactory explanation further theoretical and experimental investigation is necessary.

IV. NUMERICAL RESULTS

Figure 2 shows numerically calculated diffusive equilibrium curves for values of $C_i/C_0^{(N)}$ that are 1% of those set during the water preparations. By this we take into account

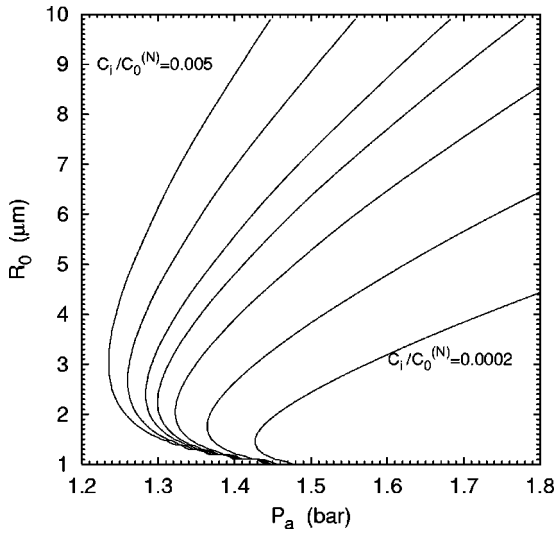

FIG. 2. Numerically calculated diffusive equilibrium curves for $C_i/C_0^{(N)}$ values corresponding to the inert gas content. The choice of $C_i/C_0^{(N)} = 0.01 \times C_i/C_0$ takes into account that a stable light emitting air bubble contains only argon. From left to right the curves correspond to $C_i/C_0^{(N)}$ values of 0.005, 0.0031, 0.002, 0.0015, 0.001, 0.0005, and 0.0002.

that in stable SL phase the bubble contains only argon. The superscript ''*N*'' distinguishes numerically calculated dimensionless concentrations from those set during the water preparation. The part of the curves with positive (negative) slope represent stable (unstable) diffusive equilibria. Note that the meta-stable points (the part of the curves with infinite slope) tend to be shifted towards higher P_a and lower R_0 values, and the stable parts of the curves get steeper as $C_i/C_0^{(N)}$ decreases. Since $R_{\max}$ increases monotonically with P_a at a given R_0, this already implies that by decreasing C_i/C_0 the expansion ratios $R_{\max}/R_0$ will grow, and thus more extreme conditions are expected within bubbles at low dissolved air concentrations, if the corresponding states are not forbidden by the onset of shape instabilities. These curves were obtained by using the approach of Brenner *et al.* [9], which is basically to calculate weighted averages over the acoustic period:

$$C_i/C_0^{(N)}=\frac{\int_0^T R(t)^4 P_g(R(t))dt}{P_0^* \int_0^T R(t)^4 dt}. \tag{1}$$

Here P_g is the uniform gas pressure inside the bubble, given by the van der Waals equation of state, modified to include the effects of surface tension σ and of vapor pressure P_v,

$$P_g(R(t))=\left(P_0+\frac{2\sigma}{R_0}-P_v\right)\frac{(R_0^3-a^3)^\gamma}{(R(t)^3-a^3)^\gamma}, \tag{2}$$

and $R(t)$ is a solution to the Rayleigh–Plesset (RP) equation [23], which governs the radius of the bubble

$$R\ddot{R}+\frac{3}{2}\dot{R}^2=\frac{1}{\rho_w}[P_g(R(t))-P_f(t)-P_0+P_v] + \frac{R}{\rho_w c_w}\frac{d}{dt}[P_g(R(t))-P_f(t)]-4\nu\frac{\dot{R}}{R}-\frac{2\sigma}{\rho_w R}, \tag{3}$$

where $P_f=-P_a\sin(\omega t)$ is the forcing pressure with angular frequency ω, P_0^* is the standard atmospheric pressure, P_0 is the ambient pressure valid during the measurements, $a=R_0/8.86$ is the hard core van der Waals radius for argon, and γ is the ratio of specific heats for the gas. The rest of the parameters appearing in the formulas are c_w, the speed of sound, ρ_w the density, and ν the kinematic viscosity of water. The material constants and the vapor pressure were chosen to match the tabular values valid at the measured water temperature (see Ref. [22] for their temperature dependence). In most of the acoustic period the gas can be considered isothermic [25], thus in our calculations we used $\gamma=1$.

A. Empirical formula for the lower SL threshold

The figures of experimental data in Refs. [7,14,12] indicate that the onset of light emission (at least within experimental uncertainty) is linked to values of P_a and R_0 which correspond to the metastable points of the diffusive equilibrium curves calculated for argon concentrations. The measurements in these references were made at air concentrations of $C_i/C_0=0.2$, 0.14, and 0.1. Assuming that this behavior holds for any $0\leqslant C_i/C_0\leqslant 0.2$ one can give an empirical formula for the gas concentration dependence of the lower SL threshold by connecting the meta-stable points on Fig. 2. We found the best fit to the numeric data in the form

$$SL_{\text{lower}}=a\cdot(C_i/C_0)^{-b}. \tag{4}$$

For the actual values of the fit parameters see Ref. [26]. It must be noted, that the validity of this prediction must break down at higher values of C_i/C_0, in the parameter region of unstable SL. For instance at $C_i/C_0=0.5$ the light emitting bubble follows the path of the parametric instability curve rather than the stable diffusive equilibrium curve with $C_i/C_0^{(N)}=0.005$, [see Fig. 1(a) in Ref. [7]].

B. Fitting technique

The new fitting technique to obtain the parameters of the bubble dynamics such as P_a, R_0 is based on the information provided by the timing of the flashes in the acoustic period and the following assumptions: (1) The dynamics of the bubble is well described by the RP equation, which is the same assumption as the Mie-scattering technique relies upon [17]. (2) In stable SL phase the bubble follows the path of the stable diffusive equilibrium (SDE) curves calculated for the inert gas concentrations. This later assumption is the direct consequence of the dissociation hypothesis, which has been confirmed experimentally by several authors using different approaches [11–13]. To describe the timing of the flashes we use the dimensionless quantity $\xi=t_f/T$, where t_f is the elapsed time between the beginning of the acoustic period (T) and the arrival of the flash. Since the light emission occurs at the instant of the minimum radius in each acoustic cycle, this fact can be used to obtain ξ numerically at given values of the parameters R_0 and P_a. We solved Eqs. (3), (2), and (1) for a wide range of R_0 and P_a and from the numerical $R(t)$ data extracted ξ, C_i/C_0^N, and $R_{\max}$ for each pair of the parameters P_a and R_0. As can be seen in Fig. 3 a pair of parameters (R_0,P_a) uniquely determines a value of ξ, and vica versa, if P_a and ξ is specified it determines uniquely the R_0. According to assumption (2) C_i/C_0^N is a constant of the motion, thus by making contour plots in the $(P_a,\xi,C_i/C_0^N)$ space at the experimentally known argon concentrations one can obtain curves in (P_a,ξ) space that are one-to-one representations of the SDE curves. This representation allows direct comparison with the experimental data, since we have the relations

$$P_a=A\cdot U_{\text{pzt}}, \quad \xi=\xi_m+B, \tag{5}$$

where the suffix ''*m*'' stands for a measured value, U_{pzt} is the monitored voltage amplitude on the PZT transmitters, A is the coefficient of proportionality, and B accounts for a possible phase shift between the monitored electric signal and the resulting acoustic pressure in the water. Parameter A was fitted individually for each set of experimental data (obtained at the same C_i/C_0), because during refilling proce-

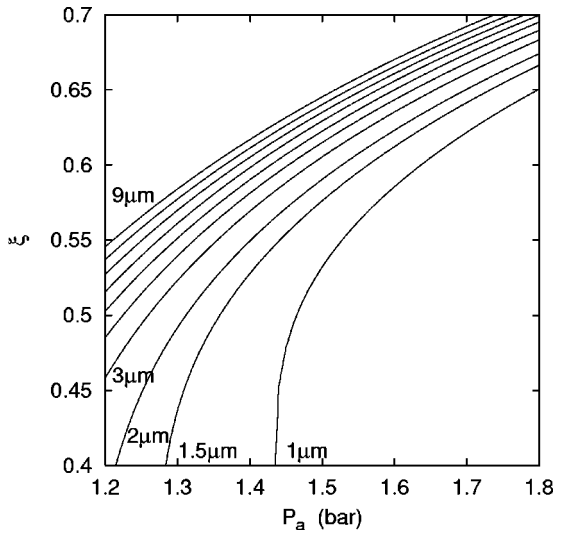

FIG. 3. The timing of the minimum radius in the acoustic cycle as a function of P_a for different values of R_0. Between $R_0=3\ \mu$m and 9 μm the increment is 1μm. The definition of ξ is given in the text.

dures the Q value of the resonator could slightly change. The other fit parameter B was assumed to be the same in all measurements, since the origin of the phase shift was electronic, which does not depend on the Q value of the resonator. Figure 4 shows that by using this approach the experimental data could be fit reasonably well to the numerically obtained SDE curves in the (P_a,ξ) plane. Near the upper thresholds the experimental data seem to deviate systematically towards lower ξ, which is equivalent with a lower R_0 (compare Fig. 4 and Fig. 3). This deviation however is not surprising if one considers that near the destruction the oscillations of the bubble are possibly no longer spherically symmetric. This would result in an increased surface and thus an excess inward gas transfer, so in order to be in diffusive equilibrium with the surrounding water the bubble has to have smaller effective R_0 (and thus a smaller ξ) at the same P_a. The fit parameters are summarized in Table I. For the relative variance of A the table gives a value around 2%, indicating that indeed the Q value of the resonator changed slightly when the water was replaced between the measurements. This sensitivity of the resonator is also confirmed by the observation that if one pushed slightly on the aluminum plates or the glass cylinder by hand, a perturbation in the light intensity could be observed. Despite this sensitivity the Q value of the unperturbed resonator can be safely considered as constant.

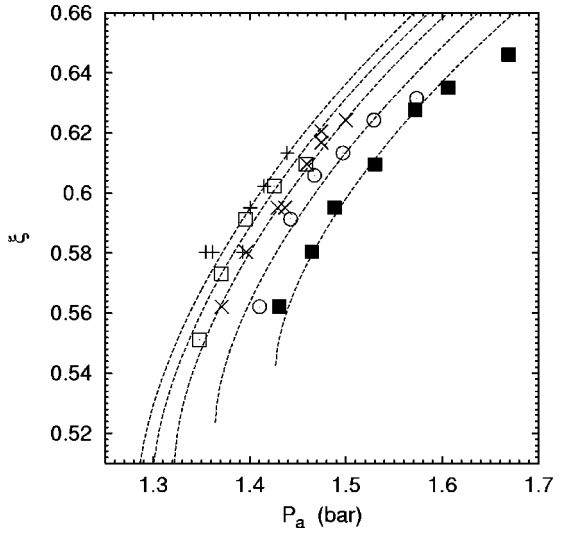

FIG. 4. Experimental data (symbols) fitted to the representations of the SDE curves in the (ξ,P_a) plane. From left to right the lines correspond to $C_i/C_0^{(N)}=0.002$, 0.0015, 0.001, 0.0005, 0.0002. The symbols are representing data measured at air concentrations of $C_i/C_0=0.2$ (pluses), 0.15 (open boxes), 0.1 (crosses), 0.05 (circles), 0.02 (filled boxes).

TABLE I. The parameters of the fit A and B for sets of data measured at different dissolved air concentrations.

$C_i/C_0^{(N)}$	B	A (bar/V)	$\langle A\rangle$ (bar/V)	$A-\langle A\rangle$ (bar/V)	$\langle\lvert A-\langle A\rangle\rvert\rangle$ (bar/V)
0.0002		2.62		0.1104	
0.0005		2.47		−0.0396	
0.001	0.303	2.525	2.5096	0.0154	0.050 48
0.0015		2.51		0.0004	
0.002		2.423		−0.0866	

Given the acoustic pressure and ξ of an experimental data point from the above fit, the corresponding R_0 parameter is uniquely determined and can be easily looked up in the calculated $(R_0,P_a,\xi,C_i/C_0^N,R_{\max})$ data. Since $R_{\max}$ is also uniquely determined by a pair of the parameters R_0 and P_a (and thus also by ξ and P_a) it can be obtained in the same way as R_0. Figure 5 shows the measured data in the (R_0,P_a) plane. The errors in P_a (not shown on the figure) are estimated by multiplying the detection error of the monitored PZT signal ($\Delta U_{\rm pzt}\approx\pm0.005$ V) by the corresponding fitting parameters A. This gives errors in P_a around 0.013 bar. The

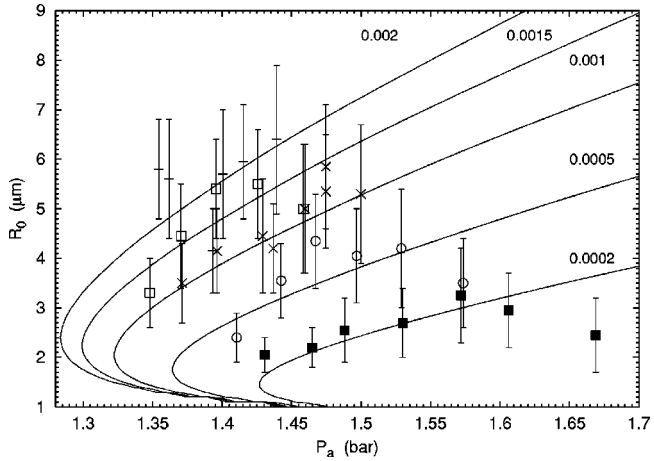

FIG. 5. Experimental data and stable diffusive equilibrium curves with $C_i/C_0^{(N)}=0.01\times C_i/C_0$ in the R_0,P_a plane. The symbols correspond to the measurements at $C_i/C_0=0.2$ (pluses), 0.15 (open boxes), 0.1 (crosses), 0.05 (circles), 0.02 (filled boxes).

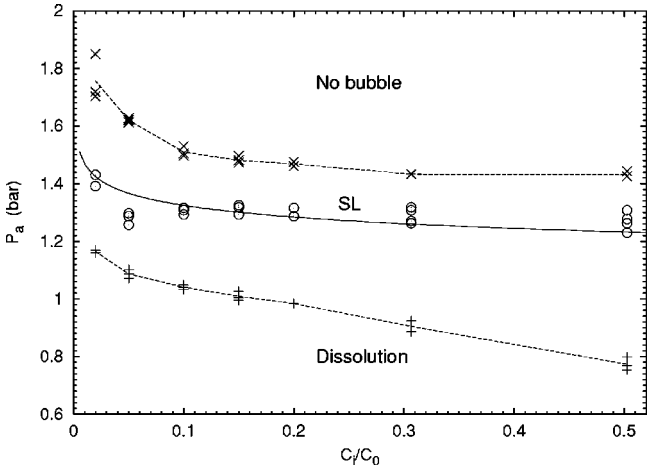

FIG. 6. Phase diagram of an air (in the SL phase argon) bubble in the $(P_a, C_i/C_0)$ plane. The dotted lines connecting the averages of data points are guides to the eye. The continuous line represents the empirical equation (4) for the lower SL threshold.

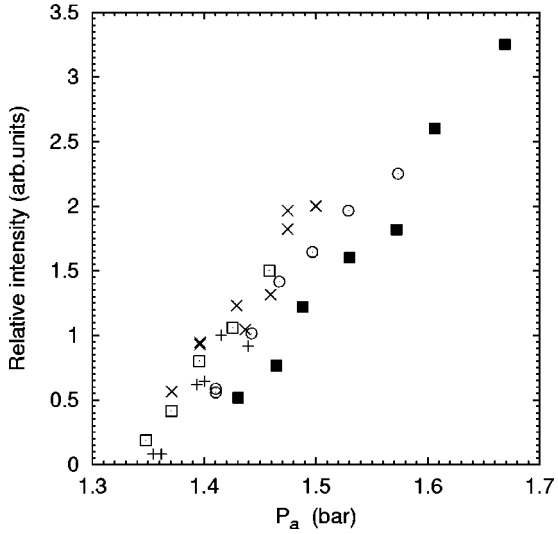

FIG. 7. Light intensity (relative to the maximum PMT signal at $C_i/C_0=0.2$) as a function of P_a, for different gas concentrations. The symbols represent the same data as in Fig. 4.

error bars of the ambient radius for a given data point were then obtained by collecting every R_0 which were allowed within the errors in P_a and ξ_m, and finding among them the smallest and biggest. ($\Delta\xi_m=\pm 0.3$ μs/42.8 μs$=\pm 0.007$). The errors in $R_{\max}$ were obtained in the same way, after which the error of $R_{\max}/R_0$ could already be calculated in a straightforward manner. We note that because of the uncertainties in the other experimental parameters the actual errors of these quantities might be slightly higher, thus our overall estimate is ± 0.03 bar for P_a and ± 1.5 μm for the ambient radius.

The data points on Fig. 5 with the highest P_a at a given $C_i/C_0^{(N)}$ define the onset of the hydrodynamic instability, which sets the upper threshold of SL. Hilgenfeldt *et al.* in Ref. [9] calculated the phase diagram of SBSL in (R_0, P_a) space, where they show that the accessible part of this parameter space is bounded from above by long and short time-scale shape instabilities. A comparison of our Fig. 5 with their Fig. 5 yields good qualitative agreement, however their shape instability curves restrict the parameter region to smaller values of R_0 and P_a than we found. At $C_i/C_0=0.2$ our data gives an upper bound on R_0 at around $6-7\,\mu$m, the same value as measured by Holt and Gaitan in Ref. [7], and also in Ref. [14].

V. PARAMETRIC DEPENDENCE

Once the parameters P_a, R_0, $R_{\max}$, and $R_{\max}/R_0$ are found for the experimental data, we can revisit our Fig. 1 and present the resulting phase diagram in the $(P_a, C_i/C_0)$ space (Fig. 6). (For the data at the two highest gas concentrations we used the average value of the fit parameter *A*, since there were no measurements done with the PMT.) The resulting P_a values for the unstable diffusive equilibrium (+), lower (○) and upper (×) SL thresholds are in good agreement with the data of Holt and Gaitan [7], as can be compared at $C_i/C_0=0.2$ and 0.5, and also with Ref. [14] at $C_i/C_0=0.14$. Note that because of the slightly higher acoustic frequency we used (23.354 kHz vs 22.6 kHz), the phase space boundaries in our case expected to lie at slightly higher pressure amplitudes, which is indeed the case. [For numerical calculations of phase diagrams in the $(P_a, C_i/C_0)$ space as a function of acoustic frequency see Fig. 19 in the recent work of Prosperetti and Hao [27], or Fig. 4 in Ref. [28] of Hilgenfeldt and Lohse.] Also good agreement is found between the experimental data of the lower SL threshold and Eq. (4), implying that it could be used for a rough calibration between the excitation signal and the resulting P_a near the bubble.

The intensity of the emitted light normalized to the maximum obtained value at $C_i/C_0=0.2$ is plotted as a function of the driving pressure amplitude in Fig. 7. Within experimental uncertainty we find a linear dependence, the same qualitative behavior as reported by several authors (see Barber and Putterman in Ref. [2], Gaitan and Holt in Ref. [14]). An interesting feature of Fig. 7 is that the data taken at different degassing levels seem to have nearly the same slope. This is surprising if one considers that the R_0 and the corresponding $R_{\max}/R_0$ parameters and their dependence on P_a (determined by the SDE curves of Fig. 2) are quite different for different values of $C_i/C_0^{(N)}$. Nevertheless these findings are consistent with the recent measurements of Ketterling and Apfel [29], who observed variations of the slope as a function of degasing for krypton and xenon bubbles, but not in the case of helium, neon, or argon.

In further investigation of parametric dependence of the light emission we checked the relative intensity divided by the ambient volume of the bubble. This quantity is proportional to the average energy emitted by a gas atom in one flash. Its dependence on the expansion ratio is shown in Fig. 8. Confirming the results of Gaitan and Holt [14] we found a power-law dependence in an extended range of the expansion ratio,

$$I_{\rm rel}/R_0^3 \sim (R_{\max}/R_0)^{3.44}. \tag{6}$$

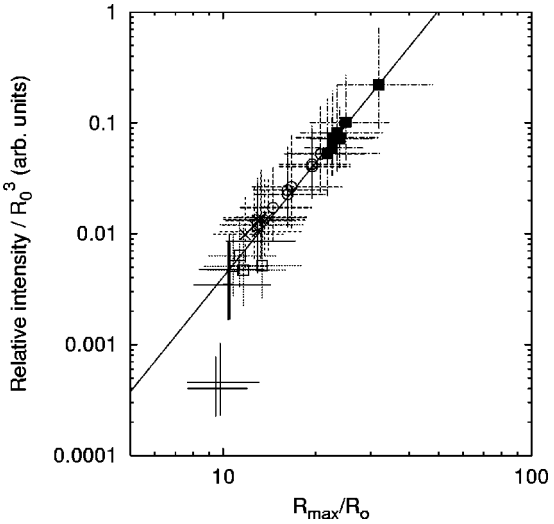

FIG. 8. Relative intensity normalized by the ambient volume of the bubble as a function of the expansion ratio for different gas concentrations. The symbols correspond to the measured data at air concentrations of $C_i/C_0=0.2$ (pluses), 0.15 (open boxes), 0.1 (crosses), 0.05 (circles), 0.02 (filled boxes).

Although our best fit produced a smaller exponent, the big errors in our data also allow for the value of 4.1, found by Ref. [14]. Note that the data obtained at different levels of degassing lie on different, almost separate parts of the curve. This indicates that the accessible conditions inside the bubble are strongly dependent on the degree of degassing, confirming the importance to control the C_i/C_0 parameter. We would like to emphasize the importance of studying the parameter region of SBSL with strong degassing, because our data suggest that the biggest expansion ratios and the most extreme internal conditions are attainable there. Note that the expansion ratios shown in Fig. 8 are consistent with previous measurements where the experimental conditions were similar to ours. Indeed the open squares of our data ($C_i/C_0=0.15$) lie in the same range between 10 and 15 as measured by Gaitan and Holt for $C_i/C_0=0.14$ [14]. For a rough estimate of the internal temperatures let us approximate the light emission with a blackbody radiation, in which case the average energy emitted by an atom in one flash can be expressed roughly as $\sim T^4\cdot\tau$, where τ is the duration of the flash. Assuming equal durations the $\sim$20-fold difference in the data in Fig. 8 predicts that roughly twice as big temperatures are attainable at a partial pressure of 15 mmHg than at 150 mmHg. This factor can be even higher if one takes into account that the flash durations tend to decrease with decreasing partial pressure, as it is clearly indicated by the measurements of Gompf *et al.* (97) in Ref. [2] and Hiller *et al.* (98) in Ref. [3]. This prediction could be tested experimentally by making spectral measurements at different levels of degassing.

VI. CONCLUSION

We performed measurements of light emission and phase diagrams of acoustically driven air bubbles, focusing on the parameter region of strong degassing with $C_i/C_0\leqslant 0.2$. A new experimental technique has been developed to obtain the parameters of the bubble dynamics $(P_a,R_0,R_{\max}/R_0)$ in the SL phase, which is based on the information provided by the timing of the flashes in the acoustic period, and the following assumptions: (1) The dynamics of the bubble is well described by the RP equation. (2) The light emitting bubbles follow the stable diffusive equilibrium curves calculated at values of C_i/C_0 corresponding to the inert gas content. Using this fitting technique we presented phase diagrams in (R_0,P_a) and $(P_a,C_i/C_0)$ planes, which are in good agreement with previous measurements, and consistent with recent theoretical models. Our findings regarding the parametric dependence of the light emission can be summarized as follows. The maximum obtainable light intensity (determined by the SL upper threshold) is found to be $\sim$3-times bigger at degassing to a partial pressure of 15 mmHg than at 150 mmHg, a different qualitative behavior as found in previous measurements of Hiller *et al.* and Chow *et al.* The difference of these results can partly be explained by the differences in the experimental apparatus and method (see Sec. III for details). As the main reason however we hypothesized that the location of the extinction threshold in the (P_a,R_0) space is not universal, but it can depend on specific experimental conditions. We believe that in order to confirm or refute this hypothesis further experimental and theoretical investigation is necessary, which would probe the sensitivity of the SL upper threshold to changes in the experimental conditions. In agreement with the measurements of Gaitan *et al.* we also found a power-law dependence of the average intensity of a gas atom on the expansion ratio. Our data suggest that the attainable conditions inside a SL bubble are more extreme at a partial pressure of 15 mmHg than at 150 mmHg. This power-law dependence can also serve as a test for SL light emission theories in a wide range of the parameter space.

ACKNOWLEDGEMENTS

The authors would like to thank Detlef Lohse, Thomas J. Matula, and Mogens T. Levinsen for valuable discussions, and Andrea Prosperetti for providing us with some of his papers. This work was supported by the Hungarian National Research Foundation, OTKA under Grant No. F025840.

[1] D. F. Gaitan, L. A. Crum, R. A. Roy, and C. C. Church, J. Am. Chem. Soc. **91**, 3166 (1992); D. F. Gaitan, Ph.D. thesis, University of Mississippi, 1990 (unpublished).

[2] B. P. Barber and S. J. Putterman, Nature (London) **352**, 318 (1991); B. Gompf, R. Günther, G. Nick, R. Pecha, and W. Eisenmenger, Phys. Rev. Lett. **79**, 1405 (1997); R. Pecha, G. Gompf, G. Nick, Z. Q. Wang, and W. Eisenmenger, *ibid.* **81**, 717 (1998); M. J. Moran and D. Sweider, *ibid.* **80**, 4987 (1998).

[3] R. A. Hiller, S. J. Putterman, and B. P. Barber, Phys. Rev. Lett.

69, 1182 (1992); R. A. Hiller, S. J. Putterman, and K. R. Weninger, *ibid.* **80**, 1090 (1998).
[4] B. P. Barber, C. C. Wu, R. Löfstedt, P. H. Roberts, and S. J. Putterman, Phys. Rev. Lett. **72**, 1380 (1994).
[5] B. P. Barber *et al.*, Phys. Rep. **281**, 65 (1997).
[6] L. Yuan, H. Y. Cheng, M.-C. Chu, and P. T. Leung, Phys. Fluids **57**, 4265 (1998); W. C. Moss *et al.*, Phys. Rev. E **59**, 2986 (1999); K. Yasui, Phys. Fluids **60**, 1754 (1999); S. Hilgenfeldt, S. Grossmann, and D. Lohse, *ibid.* **11**, 1318 (1999).
[7] R. G. Holt and D. F. Gaitan, Phys. Rev. Lett. **77**, 3791 (1996).
[8] A. Eller and H. G. Flynn, J. Acous. Soc. Am. **37**, 493 (1965); M. M. Fyrillas and A. J. Szeri, J. Fluid Mech. **277**, 381 (1994); R. Löfstedt, K. R. Weninger, S. J. Putterman, and B. P. Barber, Phys. Rev. E **51**, 4400 (1995); M. P. Brenner, D. Lohse, D. Oxtoby, and T. F. Dupont, Phys. Rev. Lett. **76**, 1158 (1996); P. H. Roberts and C. C. Wu, Theor. Comput. Fluid Dyn. **10**, 357 (1998).
[9] A. Prosperetti, Quarterly Appl. Math. **34**, 339 (1977); M. P. Brenner, D. Lohse, and T. F. Dupont, Phys. Rev. Lett. **75**, 954 (1995); S. Hilgenfeldt, D. Lohse, and M. P. Brenner, Phys. Fluids **8**, 2808 (1996); C. C. Wu and P. H. Roberts, Phys. Lett. A **250**, 131 (1998).
[10] D. Lohse, M. Brenner, T. Dupont, S. Hilgenfeldt, and B. Johnston, Phys. Rev. Lett. **78**, 1359 (1997); D. Lohse and S. Hilgenfeldt, J. Chem. Phys. **107**, 6986 (1997).
[11] T. J. Matula and L. A. Crum, Phys. Rev. Lett. **80**, 865 (1998).
[12] J. A. Ketterling and R. E. Apfel, Phys. Rev. Lett. **81**, 4991 (1998); J. Acous. Soc. Am. **107**, L13 (2000).
[13] M. Dan, J. D. N. Cheeke, and L. Kondic, Phys. Rev. Lett. **83**, 1870 (1999).
[14] D. F. Gaitan and R. G. Holt, Phys. Rev. E **59**, 5495 (1999).
[15] The motivation to study this parameter region came from our previous measurements (published in Hungarian), where we reproducibly found brighter bubbles at partial pressures less than 150 mmHg.
[16] Recently we compared the fitting technique with Mie scattering, and found that within the experimental uncertainties the two methods give identical results for P_a and R_0. Work to be published elsewhere.
[17] B. P. Barber and S. J. Putterman, Phys. Rev. Lett. **69**, 3839 (1992); R. G. Holt and L. A. Crum, J. Acous. Soc. Am. **91**, 1924 (1992).
[18] Y. J. Tian, J. A. Ketterling, and R. E. Apfel, J. Acous. Soc. Am. **100**, 3976 (1996).
[19] Subsequent measurements with a more precise instrument (JENWAY MODEL-9071 DO_2 meter, accuracy: 2%) reduced this uncertainty to 2%.
[20] R. Hiller, K. Weninger, S. J. Putterman, and B. P. Barber, Science **266**, 248 (1994).
[21] D. Chow, K. Weninger, B. P. Barber, and S. J. Putterman, J. Acous. Soc. Am. **100**, 2718 (1996).
[22] D. R. Lide, *Handbook of Chemistry and Physics*, 76th ed. (CRC, Boca Raton, FL, 1996).
[23] A. Prosperetti, L. A. Crum, and K. Commander, J. Acous. Soc. Am. **83**, 502 (1988); R. Löfstedt, B. P. Barber, and S. J. Putterman, Phys. Fluids A **5**, 2911 (1993).
[24] T. J. Matula, I. M. Hallaj, R. O. Cleveland, and L. A. Crum, J. Acous. Soc. Am. **103**, 1377 (1997); J. Holzfuss, M. Rüggeberg, and A. Billo, Phys. Rev. Lett. **81**, 5434 (1998); R. Pecha and B. Gompf, *ibid.* **84**, 1328 (2000).
[25] A. Prosperetti, J. Acous. Soc. Am. **61**, 17 (1977).
[26] The parameters of the fit are $a = 1.1946 \pm 0.0019$ bar and $b = 0.044\,85 \pm 0.000\,69$.
[27] A. Prosperetti and Y. Hao, Philos. Trans. R. Soc. London, Ser. A **357**, 203 (1999).
[28] S. Hilgenfeldt and D. Lohse, Phys. Rev. Lett. **82**, 1036 (1999).
[29] J. A. Ketterling and R. E. Apfel, Phys. Rev. E **61**, 3832 (2000).